Neural Network Application to Fault Detection by Wavelet and Coherence Analysis in Electric Motors

Serhat Şeker Emine Ayaz Erdinç Türkcan
Electrical Engineering Department, İstanbul Technical University
34469, Maslak, Istanbul-Turkey
e-mail: seker@elk.itu.edu.tr

Abstract- **This paper is based on the accelerated aging studies in electric motors and using the advanced data analyzing techniques such as wavelet and coherence analysis, the characteristic features of the motor bearings are extracted. Fault detector is designed and using auto associative neural network approach for detection of bearing damage frequencies.**

I. INTRODUCTION

The demand for monitoring and fault diagnosis of process dynamics and sensors in industrial systems has increased the efforts to develop new analysis and fault detection based on the intelligent techniques. The main goal of this technological improvement is to obtain more detailed information contained in the measured data than had been previously possible.

In literature, several studies have been conducted to identify the cause of failure of induction motors in industrial applications. More than fifty percent of the failures are mechanical in nature, such as bearing, balance and alignment related problems [1-7].

The paper presents a systematic approach to extract features from motor vibration and currents signals of 5-HP motors from load tests on motors subjected to bearing fluting or electrical aging [8]. Test data are processed to assess the effect of bearing fluting in each aging cycle of the induction motor by using multi-resolution wavelet analysis methodology. As a result of this study, mechanical feature can be detected from the motor current and vibration signals by the wavelet analysis and then the relationship between these signals can be computed as a coherence function to teach this relationship to an auto-associative neural network. This study defines the neural network structure as a fault-detector.

II. MATHEMATICAL BACKGROUND

In this section, a short view will be given in terms of theoretical basis of Multiresolution-Wavelet Analysis (MRWA) and coherence analysis approaches.

A. A Brief Knowledge on MRWA

The Discrete Wavelet Transformation (DWT) is defined as

$$DWT[j,k] = \frac{1}{\sqrt{a_0^j}} \sum_n f[n]\,\psi\left[\frac{k - na_0^j}{a_0^j}\right] \qquad (1)$$

Where ψ is called the mother wavelet and it has two characteristic parameters, namely, dilation (a) and translation (b), which vary continuously. Here, the translation parameter, "b", controls the position of the wavelet in time. A "narrow" wavelet can access high-frequency information, while a more dilated wavelet can access low-frequency information. This means that the parameter "a" varies for different frequencies. The parameters "a" and "b" take discrete values. $a = a_0^{\,j}$, $b = nb_0 a_0^{\,j}$, where $n, j \in Z$, $a_0 > 1$, and $b_0 > 0$. S. Mallat introduced an efficient algorithm to perform the DWT known as the Multi-Resolution Wavelet Analysis (MRWA). The MRWA is similar to a two-channel sub-band coder used in high-pass and low-pass filters, from which the original signal can be reconstructed. [9-11]. Figure 1 shows the frequency decomposition of the signal schematically. The low-frequency sub-band is referred to as 'approximation a_i' and the high-frequency sub-band by 'detail d_i.' Thus, at the second stage the signal may be reconstructed as $S = a_2 + d_1 + d_2$.

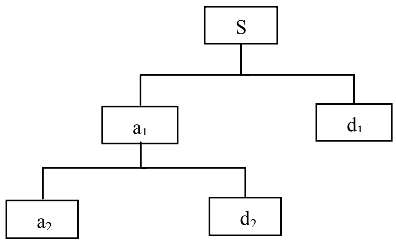

Fig.1.Signal decomposition at the second stage.

B. Spectral and Coherence Analysis

A common approach for extracting the information about the frequency features of a random signal is to transform the signal to the frequency domain by computing the discrete Fourier transform. For a block of data of length N samples the transform at frequency $m\Delta f$ is given by

$$X(m\Delta f) = \sum_{k=0}^{N-1} x(k\Delta t)\,\exp[-j2\pi km/N]. \qquad (2)$$

Where Δf is the frequency resolution and Δt is the data-sampling interval. The auto-power spectral density (APSD) of $x(t)$ is estimated as

$$S_{xx}(f) = \frac{1}{N}\,|X(m\Delta f)|^2,\; f = m\Delta f. \qquad (3)$$

The cross power spectral density (CPSD) between *x(t)* and *y(t)* is similarly estimated. The statistical accuracy of the estimate in Equation (3) increases as the number of data points or the number of blocks of data increases.

The cause and effect relationship between two signals or the commonality between them is generally estimated using the coherence function. The coherence function is given by

$$\gamma_{xy}(f) = \frac{\left|S_{xy}(f)\right|}{\sqrt{S_{xx}(f)S_{yy}(f)}}, \quad 0 < \gamma_{xy} < 1 . \qquad (4)$$

Where S_{xx} and S_{yy} are the APSD's of *x(t)* and *y(t)*, respectively, and S_{xy} is the CPSD between *x(t)* and *y(t).* A value of coherence close to unity indicates highly linear and close relationship between the two signals [12].

III. BEARING DAMAGE IN ELECTRIC MOTORS

The rotor is supported by bearings with a grease film that is not conductive. At high speeds, an even distribution of the grease film exists, and the rotor is not in contact with the outer bearing race. The rotor voltage can increase with respect to ground. When this voltage builds to a level capable of breaking down the grease film, a spark occurs and discharge mode current flows through the bearing. At low speeds, the grease film is minimized. The balls often make contact with the race. The rotor voltage does not build. The current flows through the bearing in a conductive mode. The bearing current thus has two modes, conduction and discharge. Conduction mode bearing currents exhibit continuous flow through the bearings. This form of bearing current does not result in premature bearing failure because current flows continuously without arching. Discharge mode bearing currents occur at random when the grease film momentarily breaks down. When pits caused by the electric discharge machining effect continue to occur in an operating bearing and begin to overlap, groove-like configurations called "flutes" will form. This "fluting" is the source of audible bearing noise and reduced bearing life. As a result, rolling elements and the races get damaged. This surface degradation causes extreme vibration levels of the bearing and its eventual failure.

A. Accelerated Aging Processes and Data Acquisition System

In order to simulate the electrical discharge from the shaft to the bearing, a special test setup was designed. A schematic is shown in Figure 2. The fluting run had duration of 30 minutes with the motor rotating at no load, with an externally applied shaft current of 27 Amperes at 30 Volts AC. The fluting aging is followed by thermal and chemical aging in order to increase and accelerate the aging process. After each cycle of accelerated aging, the test motor was put on a motor performance test platform. From the experimental setup, high frequency data with a sampling frequency of 12 kHz and low frequency data with a sampling frequency of 666.67 Hz were collected experimental setup and locations of the sensors related to the measurements were given in Figure 3 (a), (b) and (c) respectively. Here (5-10) sensor numbers indicate the accelerators.

IV. PRE-PROCESSING OF THE SIGNALS BEFORE NEURAL NETWORK APPLICATION

In this section, pre-processing of sensor data that is collected from the motor experimental set-up is considered. Therefore, two important procedures are aimed: a) Feature extraction procedure from the motor vibration and current signals by means of the Multi-Resolution Wavelet Analysis (MRWA). b) Coherence function between the motor current and vibration signals, where it provides the input-target pairs to be applied to Auto-Associative Neural Network (ANN) topology for training process.

A. Feature Extraction by Wavelet Analysis

The analysis of the data from bearing fluting was performed using the MATLAB 5.1 Wavelet Toolbox [13]. Several steps were performed before MRWA or the sub-band analysis. The frequency spectra of all the six accelerometer signals were computed in order to establish the vibration signal that is most sensitive to bearing fluting. The vibration signal at the process-end 2'o clock position (sensor #9), as shown in Fig.3(c), was determined as the most important signal related to the bearing fluting. The MRWA technique was applied to this measurement. Initially, the wavelet analysis requires the selection of an optimal wavelet to be used and it can be determined by its minimum energy level. For this purpose, the minimum entropy energy selection method, implemented in the MATLAB 5.1 wavelet toolbox, was executed and the optimal wavelet basis functions were selected for the vibration signals from the initial and final aging cycles. These wavelet basis functions were determined to be Daubechies-20 (db-20), and Daubechies-15 (db-15) for initial and final motor cases respectively. The sub-band or the MRWA of the two signals was performed by dividing them into eight sub-bands in the frequency range 0-6 kHz. These are given in Table 1 in terms of details (d_i) and approximations (a_i).

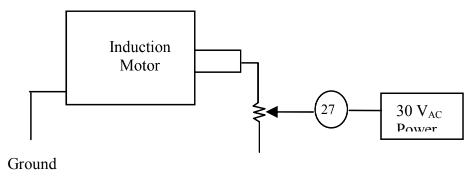

Fig. 2. Schematic of the electrical motor bearing fluting setup.

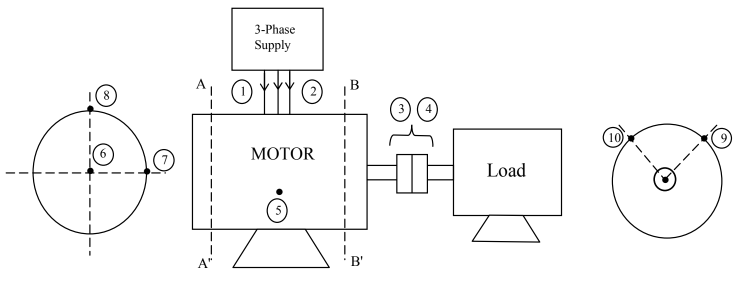

a b c

Fig.3. a) Cross Section (A-A') at Short End. b) Experimental Setup Configuration. c) Cross Section (B-B') at Process End.

Table 1.
Frequency sub-bands of the vibration signal

Approximations	Sub-bands (Hz)	Details	Sub-bands (Hz)
*a*1	0 – 3000	*d*1	3000 – 6000
*a*2	0 – 1500	*d*2	1500 – 3000
*a*3	0 – 750	*d*3	750 – 1500
*a*4	0 – 375	*d*4	375 – 750
*a*5	0 – 187.5	*d*5	187.5 – 375
*a*6	0 – 93.75	*d*6	93.75 – 187.5
*a*7	0 – 46.875	*d*7	46.875 – 93.75
*a*8	0 – 23.4375	*d*8	23.4375 – 46.875

Hence, MRWA implementation can be shown as in the following Figure 4 for final aged case

According to these results, 3-6 kHz frequency band, which is named as first detail (d_1) in MWRA, is the most dominant band in terms of the above mentioned similarity. The ratio, which can be calculated between the RMS values of vibration measurement and the RMS values of (d_1), increases as the motor bearing degrades toward failure. Hence, a feature extraction from considered data could be very effectively realized by using the multi-resolution wavelet analysis after the vibration analysis, if it is used to determine the bearing damage effect from the motor current signals. For this aim, it is examined through the combination of classical spectral analysis like short-Time Fourier Transform and Multi-Resolution Wavelet Analysis or Sub-band analysis. The result of this combination can be presented as shown in Figure 6.

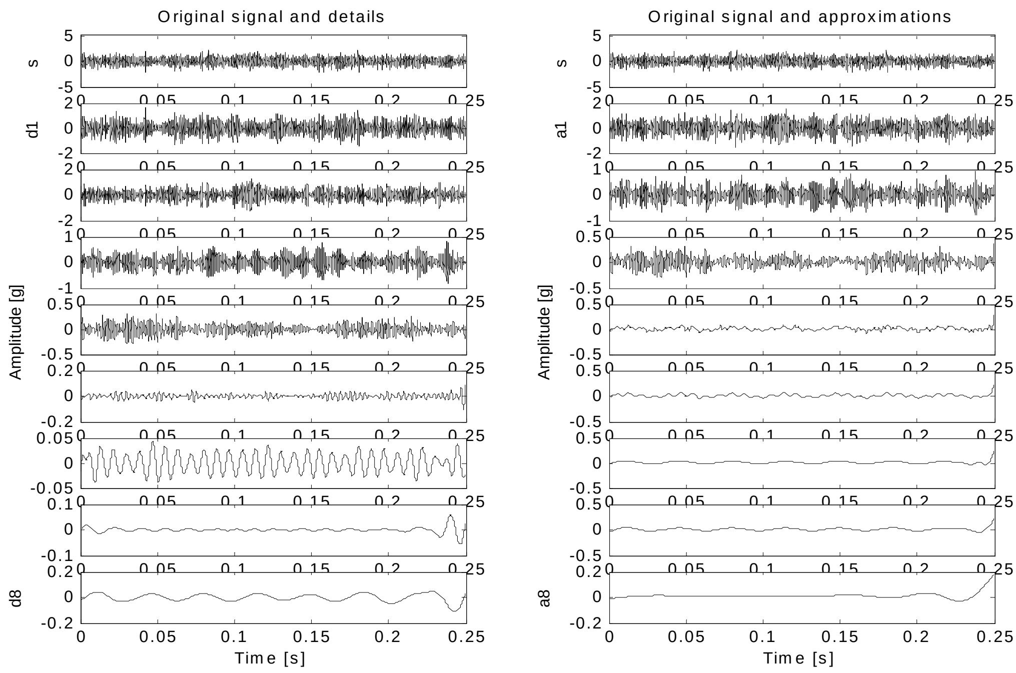

(a) (b)

Fig. 4. Details and approximations of vibration signal (s) after final aging cycle.
a) Detail sub bands ($d1$-$d8$) vibration signal (s) for aged case.
b) Approximation sub bands ($a1$-$a8$) vibration signal (s) for aged case.

A similarity was observed between the overall RMS trends of the vibration signal and overall RMS trends related to some sub-bands for each aging cycle as shown in Figure 5.

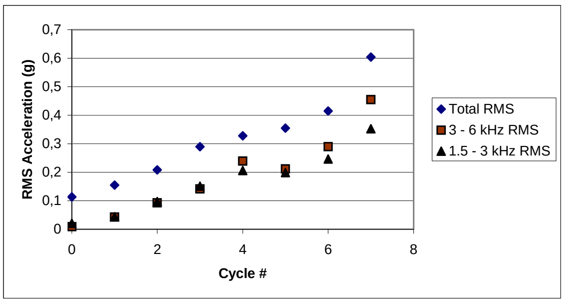

Fig.5. RMS values of vibration signal and two sub- bands (d_1 and d_2) for each aging cycle.

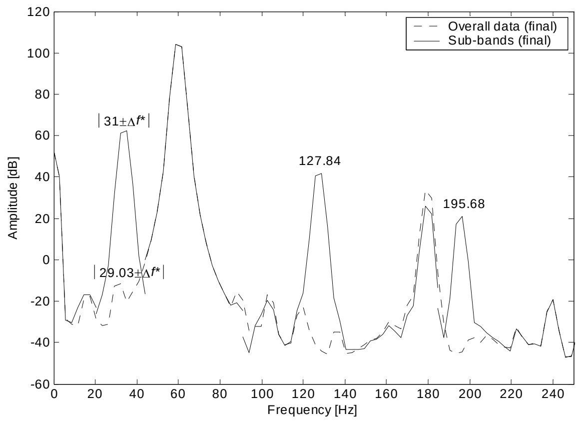

Fig.6. Original spectrum and spectrum of sub-band combination for motor current signal in final aged case.

Using the above approach, which is defined by the sub-band combination in frequency domain, it is easily observed the effect of the eccentricity frequency value at around the 30 Hz that detected from the spectral variation of the sub-band combination. Amplified effects correlated with the rotating frequency can be related to bearing damage problem in the physical sense.

Hence, the bearing damage effect can be determined by both of the motor vibration and current signals. After that the correlation function can be considered for more detailed identification of these type faults.

B. Coherence Analysis Results for Fault Identification

The relationship between bearing vibration and stator current is influenced by the air gap eccentricity, which in turn generates anomalies in the air gap flux density. Hence, the resulting field causes frequency side bands at around the supply frequency of the stator current signal for each phase. The side-band frequencies caused by the dynamic eccentricity are given as

$$f_{ecc} = f_e\left[1 \pm k\left(\frac{1-s}{p/2}\right)\right] = \left| f_e \pm k f_r \right|, \; k = 1, 2, 3, \ldots \quad (5)$$

Where f_e is the electrical supply frequency, s is the per unit slip, p is the number of poles, and f_r is the rotor speed in Hz. Slip $s = (f_s - f_r)/f_s$, where f_s is the synchronous frequency.
As a result of aging processes, bearing defect produces a radial motion between the rotor and stator of the induction motor and, the variations that are produced by the air gap eccentricity also generate stator currents that are related to the characteristic bearing frequencies (f_v) as

$$f_{bng} = \left| f_e \pm m f_v \right|, \; m = 1, 2, 3, \ldots \quad (6)$$

Sample plots of stator currents and vibration signals are shown in Fig. 7(a), 7(b) and Fig. 8(a,b) for initial and final aging cycles, respectively. According to these figures, comparing the Fig.8(a) and Fig.8(b), it is determined that there is an increase in the vibration signal amplitudes. This result may be observed from the probability density functions in Fig.8(c).

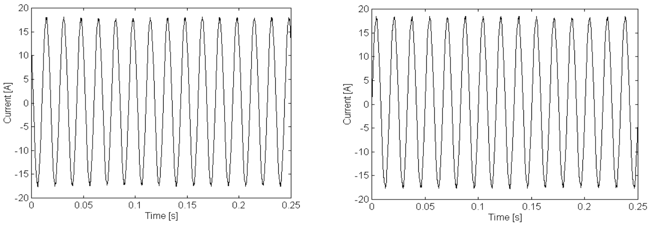

(a) (b)

Fig.7. A sample of stator currents for one phase: *a*) initial, *b*) final cycle

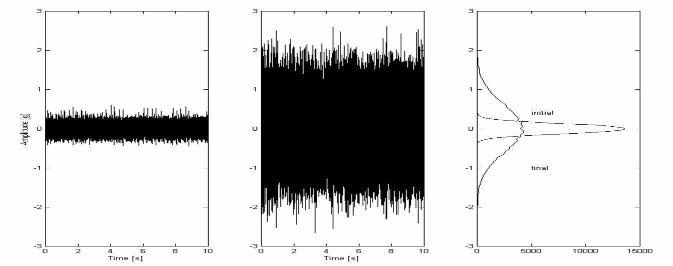

(a) (b) (c)

Fig.8. Accelerometer signal waveforms: a) Baseline. b) Final aged cycle. c) Probability density functions of a) and b).

To identify bearing damage through the motor current signal, coherence function between the motor current and vibration signature were computed and plotted in Fig. 9(a) and (b).
The coherence function plot in Fig. 9(b) indicates that the most dominant frequency values, where motor current and vibration signals are correlated, are located at 234 Hz and 469 Hz. The ball defect frequency for this bearing is calculated as f_b = 136.9 Hz using the manufacturer's catalogue values [5]. Hence, from Eq. (5) the side-band frequency due to the dynamic eccentricity is given by

$$f_{ecc} = 60 + 6(29.03) = 234 \text{ Hz}.$$

From Eq. (6) the gap eccentricity generated current due to the bearing defect is given by

$$f_{bng} = 60 + 3(136.9) = 470.7 \text{ Hz}.$$

The coherence function between the motor current and the accelerometer signals at the above frequencies has increased from the initial to the final cycle [1,5,7].

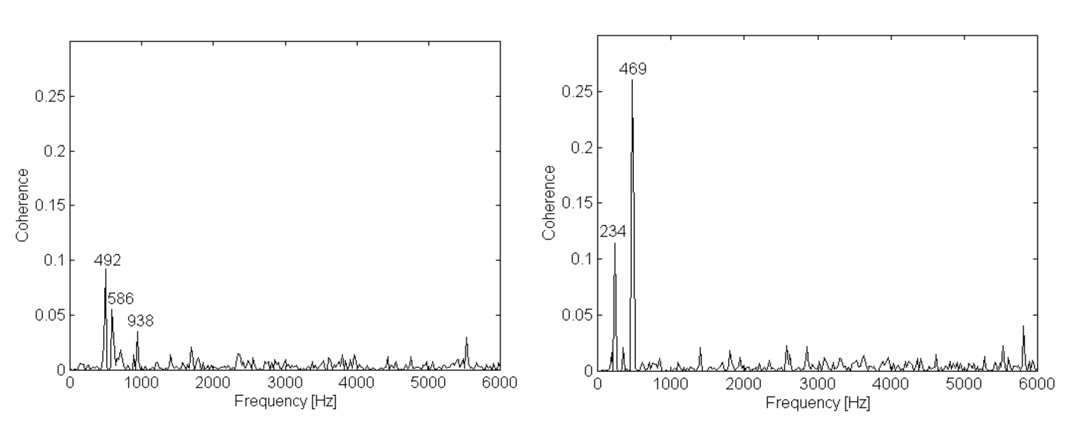

a) (b)

Fig.9. Coherence between motor current and vibration signals: a) Initial. b) Final cycle.

V. NEURAL NETWORK APPLICATION AS A FAULT DETECTOR

This case study consists of data from the pre-aging motor load tests and seven fluting aging cycles. For each aging cycle and one initial case, motor current and vibration relationship is presented in the manner of coherence function computed at 256 amplitude points between 0-6 kHz. After this, eight coherence signals are used to create the input-output pattern set of the auto-associative neural net (ANN) with one hidden layer as shown in Fig. 10. This pattern set is separated into two parts in terms of the training and recalling data sets. In the training process, learning rate of the ANN is chosen as 0.1. Here, the learning algorithm used in this application is standard back-propagation algorithm.

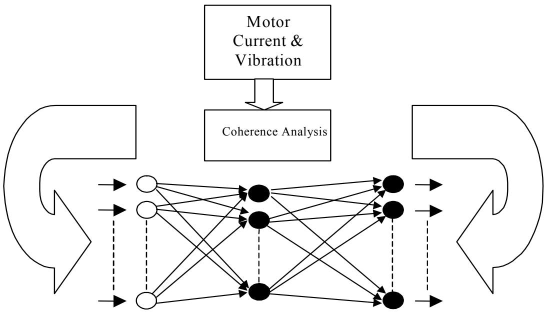

Fig.10. ANN-structure used as a fault detector.

The training data set contains the first five patterns including the initial case. Here, each input pattern is, at the same time, used as a target pattern. And the others are applied to input layer of the neural net for recalling process.

Hence, for this application, a huge topological structure of the ARNN is created with the size of 256:100:256. According to this, the bearing damage or bad bearing condition is determined by big error amplitudes observed at neural net's output nodes, which are indicated with specific frequency values, to define the motor bearing failure modes.

Also, Fig.11 shows the coherence and the error variations produced at the output layer of the ANN. In terms of the ANN-application results, special frequency at around 469 Hz, which defines the ball-defect frequency based on the air-gap eccentricity of the rotor, is easily detected by error deviation appeared at the ANN's output layer.

This is an alternative approach to some studies taken place in the related literature [14] and it is called as a fault detector based upon the soft computing technique.

VI. CONCLUSIONS

In this application, bearing damage degradation for induction electric motor of 5HP was determined by using the neural network structure trained by means of the coherence signals. In terms of the pre-processing of the related data, physical feature was extracted by the wavelet analysis both of the motor and vibration signals and the bearing damage effect was identified through the coherence analysis. Hence, special frequencies such as air gap eccentricity and its second harmonic were easily detected through the error variation occurred at the output nodes of the neural net. Also, coherence approach provides an extra advantage as the normalized data handling. After that, these determined frequency values were concluded as eccentricity frequency and ball-defect frequency values. Therefore, the ANN approach used in this study is named as an "Intelligent Fault Detector"

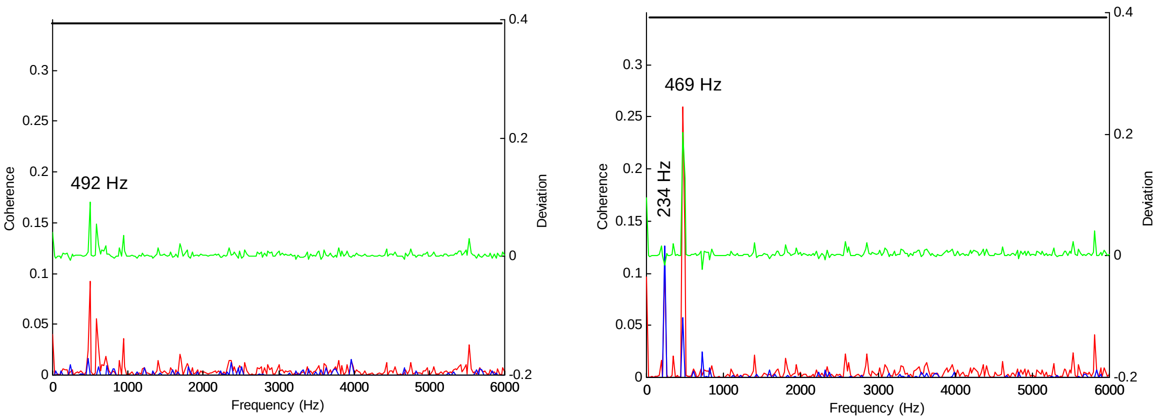

(a) (b)

Fig.11. Results of ANN: *a*) Healthy bearing case. *b*) Faulty bearing case.

REFERENCES

[1] S. Şeker, E. Ayaz, A Study on Condition Monitoring for Induction Motors Under the Accelerated Aging Processes, *IEEE Power Engineering Review*, Vol. 22, Issue 7, July 2002.

[2] S. Şeker, E. Ayaz, A Reliability Model for Induction Motor Ball Bearing Degradation, Electric Power Components & Systems, Vol. 31, No. 7, July 2003.

[3] S. Şeker, E. Ayaz, Feature Extraction Related to Bearing Damage in Electric Motors by Wavelet Analysis, *Journal of the Franklin Institute*, Vol.340, Issue 2, March 2003, pp. 125-134.

[4] R.R. Schoen, T.G. Habetler, F. Kamran and R.G. Bartheld, Motor Bearing Damage Detection Using Stator Current Monitoring, *IEEE Transactions on Industry Applications*, 31, No.6, 1274-1279, 1995.

[5] E. Ayaz, *Bearing Fault Diagnosis with the Approach of Wavelet Analysis and a Condition Monitoring System Based on Artificial Intelligence in Electric Motors*, PhD Thesis-İTÜ Institute of Science and Technology, (in Turkish) May 2002.

[6] W. J. Wang, P. D. McFadden, Application of Wavelets to Gearbox Vibration Signals for Fault detection, *Journal of Sound and Vibration* 192 5 (1996) 927-939.

[7] S. Şeker, E. Ayaz, B.R. Upadhyaya, A.S. Erbay, Analysis of Motor Current and Vibration Signals for Detecting Bearing Damage in Electric Motors, *MARCON 2000, Maintenance And Reliability Conference*, Knoxville, May 8-10, 2000.

[8] S. Şeker, B.R. Upadhyaya, A.S. Erbay, J.P. McClanahan and A.A. daSilva, Rotating Machinery Monitoring and Degradation Trending Using Wavelet Transforms, *Maintenance and Reliability Conference Proceedings*, 1, pp. 23.01-23.11, 12-14 May, Knoxville, 1998.

[9] I. Daubechies, The Wavelet Transform, Time-Frequency Localization and Signal Analysis, *IEEE Trans. on Information Theory*, 36, No.5, 1990.

[10] I. Daubechies, *Ten Lectures on Wavelets*, SIAM, Philadelphia, P.A. 1992.

[11] S. Mallat, A Theory for Multiresolution Signal Decomposition the Wavelet Representation, *IEEE Trans. Pattern Anal. And Machine Intelligence*, 11, No.7, 674-693, 1989.

[12] V.S. Vaseghi, *Advanced Signal Processing and Digital Noise Reduction*, John Wiley, New York, 1996.

[13] M. Misiti, Y. Misiti, G. Oppenheim, J.M. Poggi, *Wavelet Toolbox for use with MATLAB*, The Math Works, Inc. 1996.

[14] Gao, X.Z., Ovaska, S.J., 2000. Motor fault detection using Elman neural network with genetic algorithm-aided training. *IEEE International Conference on Systems, Man, and Cybernetics* 4, 2386-2392.